Supporting Information:

Single-unit-cell thick Co_9S_8 nanosheets from preassembled Co_{14} nanoclusters

Zhennan Wu, Haoyang Zou, Tingting Li, Ziyi Cheng, Huiwen Liu, Yi Liu, Hao Zhang, and Bai Yang*

Z. N. Wu, H. Y. Zou, T. T. Li, Z. Y. Cheng, H. W. Liu, Dr. Y. Liu, Prof. H. Zhang and Prof. B. Yang
State Key Laboratory of Supramolecular Structure and Materials, College of Chemistry, Jilin University, Changchun 130012, P. R. China.
E-mail: hao_zhang@jlu.edu.cn

Experimental Section

Materials. 1-Dodecanethiol (DT, 98%) was purchased from Aladdin Chemistry Co. Ltd.. Dibenzyl ether (BE, 98%) and Nafion solution (5 wt%) were purchased from Aldrich. Cobalt (II) acetylacetonate ($CoAc_2$) was purchased from Alfa. Aesar. KOH, H_2SO_4, NaH_2PO_4 buffer solution (pH=6.7), isopropanol, acetone, and chloroform were all commercially available products and used as received without further purification.

Preassembly of $Co_{14}DT_9$ NCs. 30 mg (0.12 mmol) $CoAc_2$ was dissolved in 10 mL BE at room temperature. 1 mL (4 mmol) DT, which acted as ligand *cum* reductant, was added into the mixture and stirred at 120 ºC for 30 min to produce the preassembled architectures of $Co_{14}DT_9$ NCs.

Purification. After cooled down to room temperature, the preassembled $Co_{14}DT_9$ architectures were washed and precipitated through the addition of 10 mL chloroform and 10 mL acetone for three times at room temperature. Separated by centrifugation, the precipitates were collected and further placed in vacuum oven at 60 ºC for 30 min to produce dried samples.

Preparation of single-unit-cell thick Co_9S_8 nanosheets. Single-unit-cell thick Co_9S_8 nanosheets were prepared from the preassembled $Co_{14}DT_9$ NCs. By annealing treatment of 20 mg preassembled $Co_{14}DT_9$ NCs combined with additional 0.1 mL DT at 400 ºC for 2 h in tube furnace under N_2 protection, 9.5 mg Co_9S_8 nanosheets were obtained. The yield is over 95%.

Characterization. Transmission electron microscopy (TEM) was conducted using a Hitachi H-800 electron microscope at an acceleration voltage of 200 kV with a CCD camera. Atomic force microscope (AFM) tapping mode measurements were performed on a Nanoscope IIIa scanning probe microscope (Digital Instruments) using a rotated tapping mode etched silicon probe tip. An energy-dispersive X-ray spectroscopy (EDS) detector coupled with scanning electron microscope (XL 30 ESEM FEG Scanning Electron Microscope, FEI Company) was used for elemental analysis. X-ray powder diffraction (XRD) investigation was carried out on a Rigaku X-ray diffractometer using Cu K radiation (λ=1.5418 Å). X-ray photoelectron spectroscopy (XPS) was investigated using a VG ESCALAB MKII spectrometer with a Mg Kα excitation (1253.6 eV). Binding energy calibration was based on C 1s at 284.6 eV. Thermogravimetric analysis (TGA) and differential thermal gravity (DTG) was carried out using Thermogravimetric Analyzer Q500 of American TA co.. Matrix-assisted laser desorption/ionization time-off light (MALDI-TOF) mass spectra (MS) were recorded on a Bruker/Auto Reflex III mass spectrometer (Bremen, Germany) equipped. The ions were accelerated with pulsed ion extraction by a voltage of 19 kV and detected using a microchannel plate detector. Samples were dissolved in THF and 2, 5-dihydroxybenzoic acid was used as the matrix material.

Electrochemical measurements. Bare glassy-carbon electrode (GCE, 3.0 mm in diameter) was treated as follows. Prior to use, the electrodes were polished mechanically with aluminite powder under an abrasive paper to obtain a mirror-like surface, washed with ethanol and de-ionized water by sonication for 5 min, and allowed to dry in a desiccator. Electrochemical experiments were conducted using AFMSRCE advanced electrochemical system of Pine-company. A conventional three-electrode cell was employed incorporating a working electrode, an Ag/AgCl electrode as reference electrode, and a Pt electrode as counter electrode. 4 mg of grinded catalysts mixed with 35 μL Nafion

solution were dispersed in 1 mL of water/isopropanol solution with the volume ratio of 3:1 by sonicating for 30 min to form a homogeneous ink. And then, 5 μL ink (0.02 mg) was dropped onto the GCE. The polarization curves were recorded with the scan rate of 5 mV s^{-1} in O_2-saturated 0.1 M KOH, 0.5 M H_2SO_4 solution, and pH=6.7 NaH_2PO_4 buffer solution for the OER. With respect to the photoelectrocatalytic OER performance, the white light illumination using 300 W xenon lamp was used during the regular electrocatalytic OER testing. All of the potentials were calibrated to a reversible hydrogen electrode according to the Nernst equation.

Figure S1. Optical (a) and microscope (b) photos of the architectures of preassembled $Co_{14}DT_9$ NCs. The assemblies are made of ultra-long nanowires.

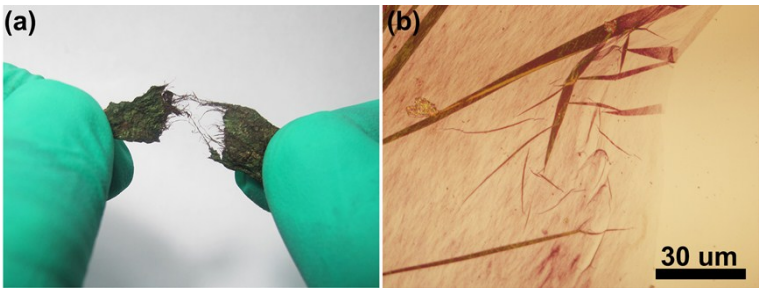

Figure S2. TGA (a) and DTG (b) data of the preassembled $Co_{14}DT_9$ NCs. The weight increase before 200 ºC is attributed to N_2 adsorption, which is led from the sponge-like structure of NCs assemblies. The final weight loss is 71%. The calculated S/Co molar ratio is 9/14.

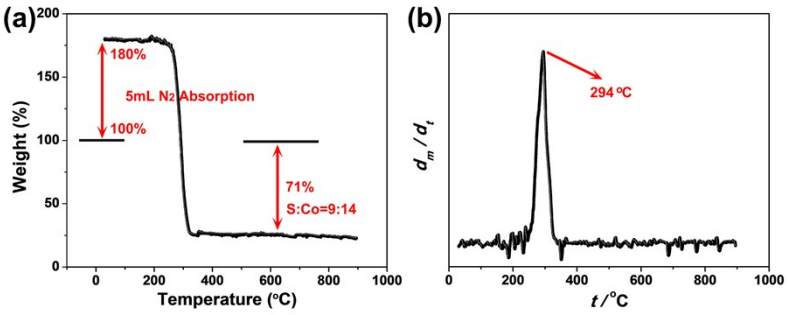

Figure S3. (a) TEM image of the preassembled $Co_{14}DT_9$ NCs, which presents the building blocks are individual NCs. (b) The size distribution of $Co_{14}DT_9$ NCs shows the average diameter of 1.8 nm.

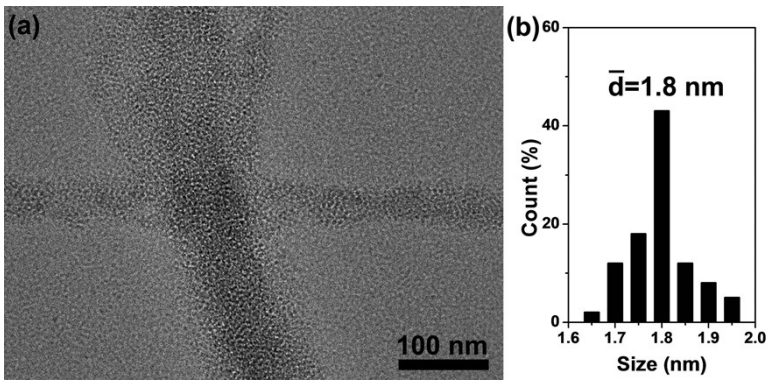

Calculation S1. Detail for the calculation of the energy of dipolar attraction. The energy of dipole attraction between $Co_{14}DT_9$ NCs can be calculated according to the classical formula for aligned dipoles $E = -\mu^2 / 2\pi\varepsilon_0 r(r^2 - d_{NC}{}^2)$. As to the dipole moment μ = 10.82 D, the center-to-center interdipolar separation r = 3.5 nm, and the diameter d_{NC} = 1.8 nm, the calculated energy of dipolar attraction is 3.9 kJ/mole.

Figure S4. The Brownian dynamics simulation confirms that the permanent dipole of $Co_{14}DT_9$ NCs is the main driving force to conduct the 1D-oritated self-assembly.

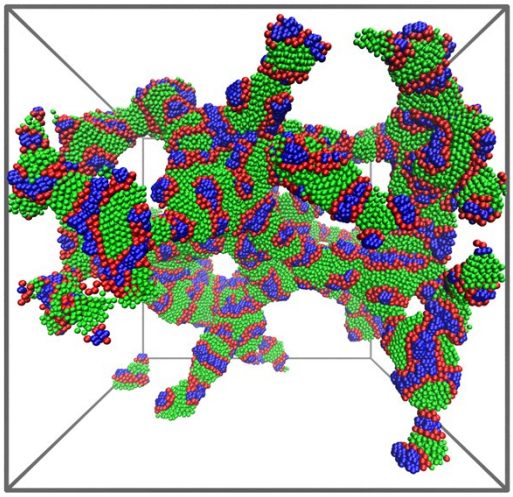

According to the molecular weights and the bulk densities of the pure species in experiments, the volumes of the monomers can be obtained. We group a sulfur, one Ac molecule and four carbon chain (-CH_2-CH_2-CH_2-CH_2- or -CH_2-CH_2-CH_2-CH_3) into one CG bead. 9 DT chains connect to a center Co is adopted to form the composite system of $Co_{14}DT_9$, where Co_{14} represents 14 CG beads that form a spherical rigid body [1].

In Brownian dynamics, the equation of motion of each bead in the system is governed by Langevin equation,

$$m_i \ddot{r}_i(t) = F_i^C(r_i(t)) + F_i^R(t) - \gamma_i v_i(t)$$

where v is the velocity of the bead, $\gamma = k_B T / D$ is the friction coefficient, and D is the diffusion coefficient. We assume that there are no spatial or temporal fluctuations of friction coefficient and fix $\gamma = 1.0$. The effect of solvents is implicitly treated by the random force which satisfies the fluctuation dissipation theorem,

$$\left\langle F_i^R(t) F_j^R(t') \right\rangle = 6\gamma k_B T \delta_{ij} \delta(t - t')$$

where k_B is the Boltzmann constant and T is the temperature. The coupling between friction and random forces acts as an effective thermostat. The simulations are performed in an NVT ensemble in a cubic box under periodic boundary conditions.

The non-bonded interactions between the coarse-grained beads are represented by Lennard-Jones (LJ) potential,

$$U_{LJ}(r) = \begin{cases} 4\varepsilon\left[(\frac{\sigma}{r})^{12} - (\frac{\sigma}{r})^{6}\right], & r \le r_{cut,LJ} \\ 0, & r > r_{cut,LJ} \end{cases}$$

in which ε and σ are the well depth and the bead diameter, respectively. r is the distance between two beads, and $r_{cut,LJ} = 2.5\sigma$ is the cutoff distance beyond which the LJ potential is equal to 0. For simplicity, all the beads in the system have the same size σ and mass m. The time unit is $\tau = \sigma\sqrt{m/\varepsilon}$. All the parameters used in this work are in reduced units with basic units being ε, σ, m, and τ. We fix $\varepsilon_{Co\text{-}Co}$ = 4.0 to describe the effective interactions between the Co beads, and $\varepsilon_{Co\text{-}S} = \varepsilon_{S\text{-}S} = \varepsilon_{S\text{-}C} = \varepsilon_{C\text{-}C}$ =1.0 to describe the interaction between the Co/S, S-C, C-C bead and the S, C beads.

$$U_{LJ}(r) = \begin{cases} U_{LJ}(r) - U_{LJ}(r_{cut,WCA}), & r \le r_{cut,WCA} \\ 0, & r > r_{cut,WCA} \end{cases}$$

in which $r_{cut,WCA} = \sqrt[6]{2}\sigma$ is the cutoff distance beyond which the WCA potential is equal to 0. We fix $\varepsilon_{Co\text{-}C} = \varepsilon_{C\text{-}S}$ =1.0 to describe the interaction between the Co/C bead and the DT beads.

Polymers are constructed by connecting adjacent beads in the chain together via harmonic spring $\vec{F}_{ij}^{S} = -k\vec{r}_{ij}$, where $k = 4$. A time step of $\delta t = 0.005$ is used, and the total simulation steps are 10^7. All simulations are performed in NVT ensemble using GALAMOST[3] on Nvidia Tesla C2050 GPU.

[1] T. D. Nguyen, C. L. Phillips, J. A. Anderson, S. C. Glotzer, *Computer Physics Communications* **2011**, *182*, 2307-2313.

[2] A. K. Rappe, C. J. Casewit, K. S. Colwell, W. A. Goddard, W. M. Skiff, *Journal of the American Chemical Society* **1992**, *114*, 10024-10035.

[3] Y.-L. Zhu, H. Liu, Z.-W. Li, H.-J. Qian, G. Milano, Z.-Y. Lu, *Journal of Computational Chemistry* **2013**, *34*, 2197-2211.

Calculation S2. Detail for the calculation of vdW attraction between neighboring $Co_{14}DT_9$ NCs.

In detail, the vdW interaction between atoms and/or molecules is expressed as the well-known formula:

$$U_{vdw}(r) = -C_{vdw} / r^6$$

where C_{vdw} is a constant characterizing the interacting species and the surrounding medium, r is the distance between atom and/or molecule center. The simplest approach to estimate the macroscopic vdW attraction between two nano-objects composed of many atoms/molecules is a pairwise summation (or integration) of these molecular interactions throughout the volume of two bodies, which results in the following approximation for two spheres with radii a_1 and a_2 separated by a center-to-center distance *r*:

$$U_{vdw}(r) = \frac{A}{3}\left[\frac{a_1 a_2}{r^2-(a_1+a_2)^2} + \frac{a_1 a_2}{r^2-(a_1-a_2)^2} + \frac{1}{2}\ln\left(\frac{r^2-(a_1+a_2)^2}{r^2-(a_1-a_2)^2}\right)\right]$$

here, A is the Hamaker coefficient and can be estimated according to the Hamaker integral approximation of $A = C_{vdW}\pi^2 / v_1 v_2$, where v_i is the molar volume of material i. For -CH_2- group, $A \approx 5\times10^{-20}$ J ($C_{vdw} \approx 50\times10^{-79}$ Jm^6, $v \approx 30$ Å^3), r is 0.527 nm corresponding to the sum of normal CH_2-CH_2 distance along alkyl chain and cylinder diameter ($2a$) composed of -CH_2- which is 0.127 and 0.40 nm, respectively. With the consideration of hexagonal alignment of the $Co_{14}DT_9$ NCs inner wires, the vdW attraction between neighboring $Co_{14}DT_9$ NCs is calculated to be 4 k_BT.

Figure S5. TEM image of the ultrathin Co_9S_8 nanosheets, which clearly shows the single-layer thickness of 0.99 nm.

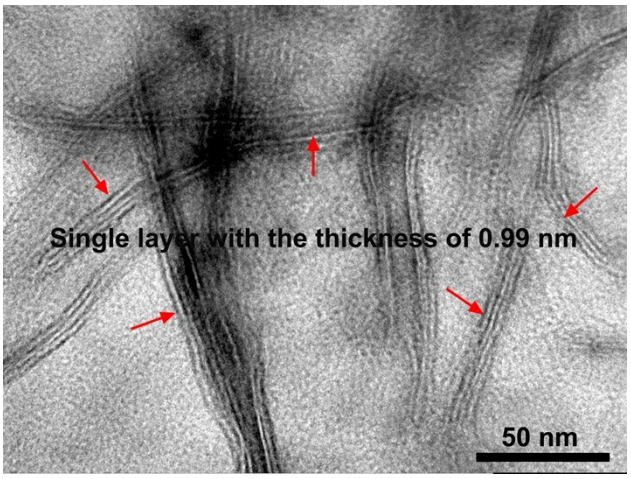

Figure S6. AFM image of the ultrathin Co_9S_8 nanosheets, which presents the minimum thickness of 0.99 nm. Besides, the thickness of 1.33 nm and 1.64 nm are also detected with a gradient change around 0.33 nm, which is equal to the thickness of single-layer C atom.

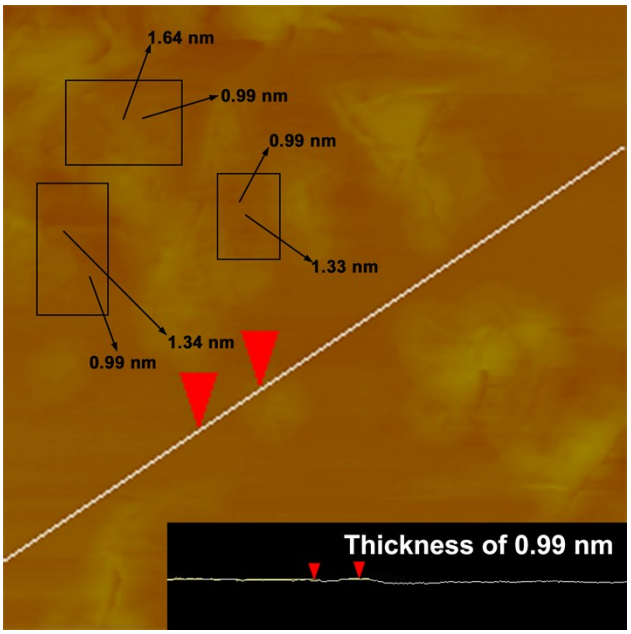

Figure S7. Top (a) and side (b) view of crystal structure of the single-unit-cell thick Co_9S_8 nanosheets.

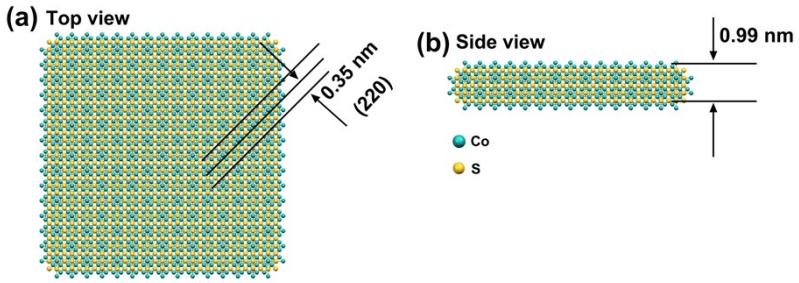

Figure S8. XPS spectrum of the ultrathin Co_9S_8 nanosheets, which shows a strong C signal besides O, S, and Co signals.

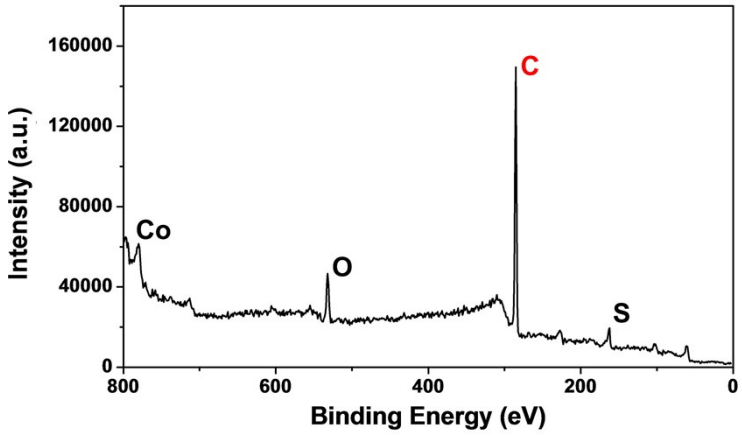

Figure S9. EDS line scan image of the ultrathin Co_9S_8 nanosheets and corresponding cross-sectional compositional line profiles, from which C signal can be detected.

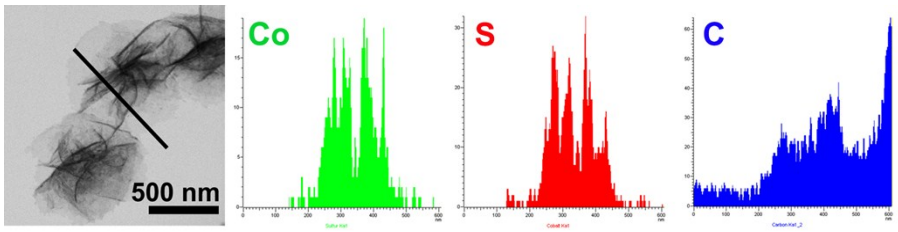

Figure S10. HRTEM image of the ultrathin Co_9S_8 nanosheets, which clearly reveals the lattice fringes of 0.34 nm in the edge area. It is assigned to the graphite-like carbon structure (002, $2\theta=25^{o}$).

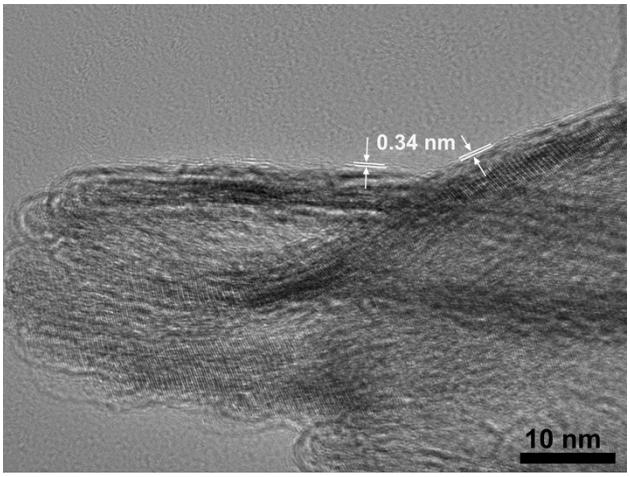

Figure S11. Optical images of the chloroform solution (a), and solid powder (b) of ultrathin Co_9S_8 nanosheets after two months storage in air at room temperature. (c) TEM image of ultrathin Co_9S_8 nanosheets after two months storage.

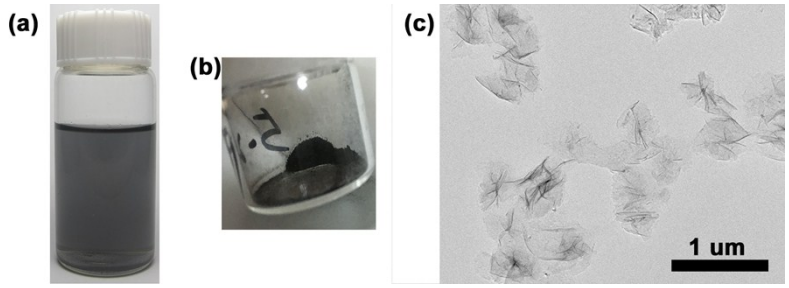

Figure S12. EDS analysis of the composition of small Co_9S_8 nanosheets obtained after 0.5 h annealing treatment of preassembled Co NCs at 400 ^oC, which reveals the distinct C signal with 32% proportion.

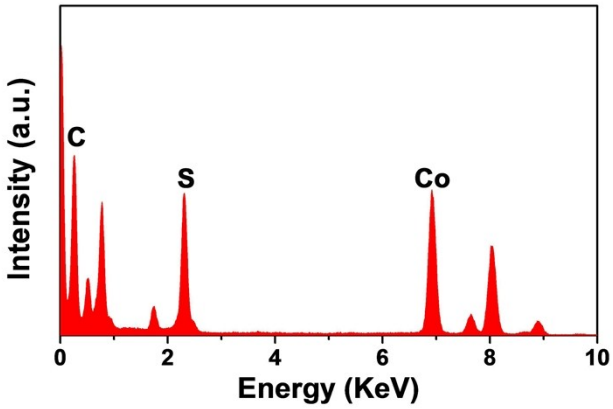

Figure S13. TEM images of the as-prepared Co_9S_8 nanocrystals with the H_2S concentration of 0.5 mmol/L (a), 1 mmol/L (b), 1.5 mmol/L (c), 3 mmol/L (d), 5 mmol/L (e), and 6.45 mmol/L (f). Ultrathin Co_9S_8 nanosheets are produced under high H_2S concentration of 6.45. In contrast, Co_9S_8 nanoparticles with the average diameter of 10 nm (a) and 20 nm (b) are obtained under low H_2S concentration. Accompany with the increased H_2S concentration (c-e).

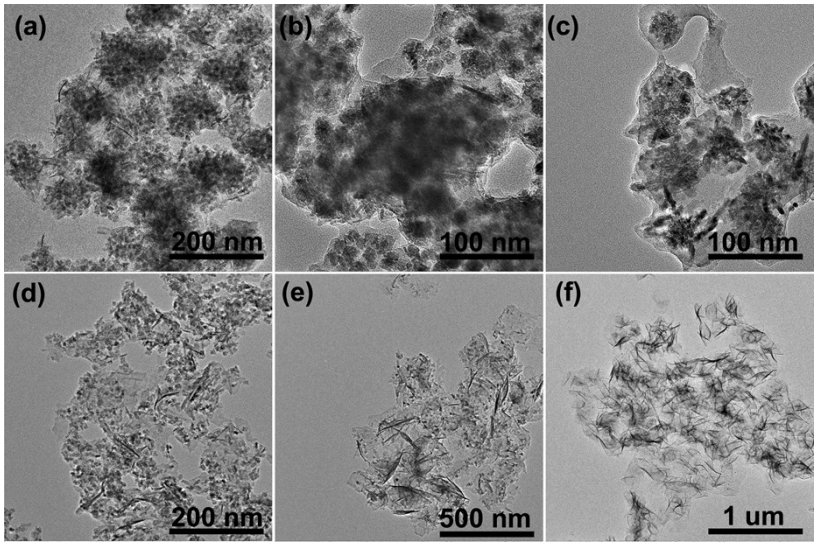

Figure S14. TEM image of the ultrathin Co_9S_8 nanosheets after 1000 cycles cyclic voltammogram test in 0.1 M KOH aqueous solution.

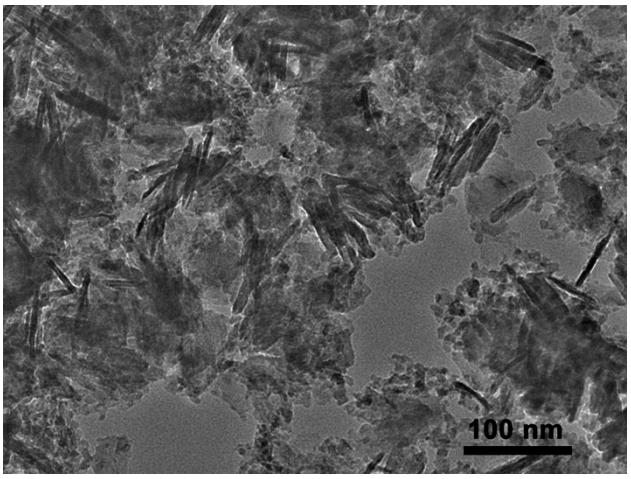

Figure S15. Polarization curves of ultrathin Co_9S_8 nanosheets before and after cyclic voltammogram test for 1000 cycles in 0.5 M H_2SO_4 aqueous solution (a), and pH=6.7 NaH_2PO_4 buffer solution (b).

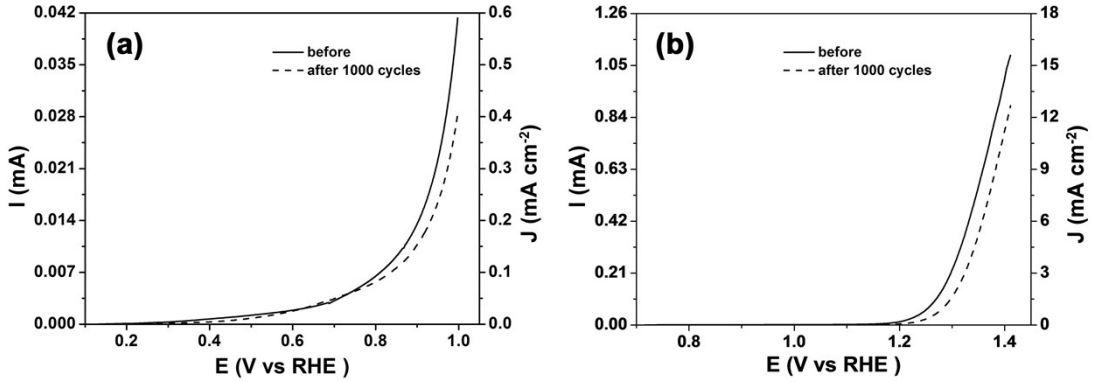

Figure S16. Polarization curves of ultrathin Co_9S_8 nanosheets with and without white light illumination using 300 W xenon lamp in 0.1 M KOH aqueous solution for OER.